separations

MDPI

Article

Study on Separation Density of Feeding Group Particle in the Gas–Solid Separation Fluidized Bed

Xuchen Fan [1,2,*], Yuping Fu [1,2,*], Yongliang He [1,2], Liying Sun [1,2] and Yijiang Li [3]

[1] School of Safety and Emergency Management Engineering, Taiyuan University of Science and Technology, Taiyuan 030024, China
[2] Intelligent Monitoring and Control of Coal Mine Dust Key Laboratory of Shanxi Province, Taiyuan University of Science and Technology, Taiyuan 030024, China
[3] School of Mechanical Engineering, Taiyuan University of Science and Technology, Taiyuan 030024, China
* Correspondence: fanxuchen@tyust.edu.cn (X.F.); 2011014@tyust.edu.cn (Y.F.)

Abstract

Gas–solid separation fluidized bed is an efficient coal cleaning and separation technology, and this technology has been extensively used in coal separation. The separation of the feeding coal particles in the fluidized bed is generally carried out in the form of particle groups, hence, a systematic examination of stratification as well as diffusion of the feeding particle group in the gas–solid separation fluidized bed is required. Simulated particles are used in this study and the technique that combines both theoretical calculation and an experimental method is used to investigate the effect of the inherent properties of the feeding particle group, bed characteristics, and operating parameters on the variation in voidage and air drag force in the separation process. According to the correlation between the separation density of the single-component particle group and the voidage of the gas–solid separation fluidized bed, the $\rho_{G.drag}$ (change in separation density brought about by the upward airflow drag force during particle group fluidized bed separation) prediction model of the single-component spherical feeding particle group in the gas–solid separation fluidized bed is developed with the correction of voidage. When the prediction error of the $\rho_{G.drag}$ prediction model is 10%, the confidence degree is 90.00%. Based on the particle segregation model and the $\rho_{G.drag}$ prediction model, the separation density prediction model for the single-component spherical feeding particle group in the gas–solid separation fluidized bed is proposed. On this basis, the separation density prediction model for the single-component non-spherical feeding particle group in the gas–solid separation fluidized bed is further introduced. The separation density prediction model provides critical guidance for optimizing the gas–solid fluidized bed separation process.

Keywords: feeding particle group; fluidized bed; separation density; voidage

Check for updates

Academic Editor: Guojie Zhang

Received: 4 December 2025
Revised: 24 December 2025
Accepted: 24 December 2025
Published: 26 December 2025

Copyright: © 2025 by the authors. Licensee MDPI, Basel, Switzerland. This article is an open access article distributed under the terms and conditions of the Creative Commons Attribution (CC BY) license.

1. Introduction

As the major fossil source of energy worldwide, coal has never occupied a lesser role in the global energy landscape, which affects the world energy landscape and economic growth with a major impact [1–4]. China made a direct announcement of its strategic plan of "dual-carbon" in September 2020 [5–8]. This strategy will speed up carbon emission mitigation and increase the effectiveness of clean coal use. It is conducive to green technological innovation and bolstering the global competitiveness of industries and the economy.

According to data from 2024, the national production of raw coal has reached 4.78 billion tons, and the rate of washing raw coal has reached 68.0 and has consistently remained

at a historically high level [9]. It is also worth noting that the coal deposits of China are mostly found in arid areas with water deficits. Consequently, the gas–solid separation fluidized bed technology with its water-saving nature has gained significant research impetus in the sphere of clean coal separation. The application of this technology makes use of airflow to push dense medium to create a uniform and stable layer of gas–solid fluidized bed, which allows the separation of coal to occur effectively by density. It is also most applicable in coal cleaning separation where there is a lack of water.

The actual separation process in the gas–solid fluidized bed is extremely complex and involves numerous influencing factors. Exploring the impact of various influencing factors on the actual separation process and identifying the suitable optimal conditions and adjustment ranges holds great value for efficient fluidized dry separation. J. Oshitani et al. found that the separation behavior of feed mineral in fluidized bed is primarily influenced by the gas velocity, bed height, feeding mineral size, and dense medium size [10–13]. Wang et al. characterized the diffusion and stratification patterns of particles from a microscopic perspective using simulation methods [14–16]. Sahu A.K. et al. further investigated the influence of the particle density, particle size, and particle shape on the particle residence position [17]. Luo et al. analyzed the forces acting on coal particles in fluidized bed and compared the difference in forces experienced by coarse and fine particles in fluidized bed [18]. In addition to gravity and buoyancy, gas and particles also experience an interaction force, or drag force, during their motion. Currently, research primarily focuses on the dispersed fluidization of dilute-phase particles, with less attention paid to the study of particle groups in dense-phase gas–solid fluidized bed with lower voidage [19–21].

Coal separation in fluidized bed generally occurs in the form of particle groups, yet group stratification and the diffusion behavior of feeding particle groups in fluidized gas–solid separation have hardly been investigated. Once the particle group enters the gas–solid separation fluidized bed, the particles disturb the flow field within the bed. Unlike the change in the drag coefficient of the fluidized bed when a single particle is introduced, the interaction between particles in the feeding particle group has a more complex impact on the distribution of feeding particles. To elucidate the pattern of particle separation, voidage serves as a crucial indicator for investigating energy conversion and transfer, bed stability, and separation efficiency in the fluidized bed. Gidaspow et al. and Bai et al. have both provided models that correct the drag coefficient of particle groups based on voidage, using the drag coefficient of individual particles as a foundation [22,23]. However, neither of the studies has addressed the need to correct for variations in the separation density of the fluidized bed that arise from the drag effect of the ascending gas flow during the process of particle selection. This study will employ a predictive model for particle separation between the feeding particle group and the dense medium, aiming to derive the relationship between the study and density influenced by the gas drag force, and thereby uncover the separation and diffusion mechanisms of particle groups within the gas–solid separation fluidized bed.

2. Materials and Methods

2.1. Apparatus and Dense Medium

The previous study [24] introduced the composition of the gas–solid fluidized bed separation system and distribution of the dense medium.

In this study, the fluidized bed gas–solid separation system consists of an air distributor, air distribution chamber, and dense medium. The fluidized bed has an inner diameter of 200 mm, a height of 350 mm, and is made of organic glass. The magnetite powder with a particle size between 0.074 and 0.3 mm is used as dense medium. The air pressure is 0.2 MPa.

2.2. Properties of Simulated Feeding Particles

The simulated feeding particles are spherical particles, with their density and particle size distribution shown in Figure 1. The densities are 1.8, 1.9, 2.0, 2.1, 2.2, and 2.3 g/cm^3, with particle sizes of 10, 15, 20, 25, 30, and 35 mm, respectively. The number of simulated feeding particles is controlled between 5 and 30.

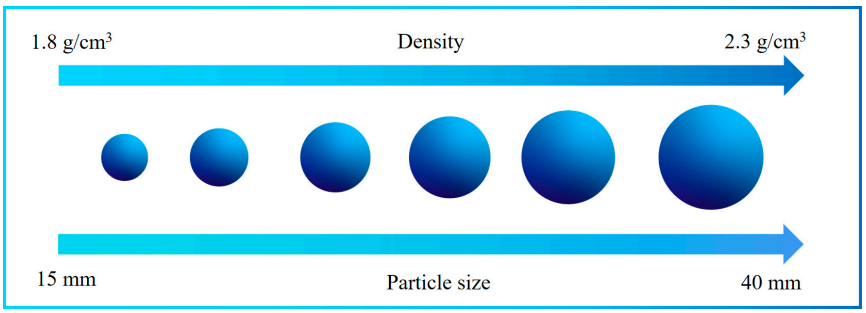


Figure 1. Properties of simulated feeding particle group.

3. Theoretical Analysis of Feeding Group Particle Separation Process

The separation behavior of particle groups in the gas–solid separation fluidized bed is illustrated in Figure 2. Compared to single-particle separation, the number of particles in the group increases when multiple particles are introduced. Due to the variations in number, size, and density within the particle group, unique distribution characteristics are formed. Under the synergistic effect of the introduced particle group and the dense medium, the bed voidage changes. Meanwhile, the bed voidage also affects the drag force exerted on the introduced particle group during separation. Therefore, based on the single-particle separation $\rho_{SS.drag}$, the density variation law of the particle group during introduction needs to be corrected according to the voidage variation law.

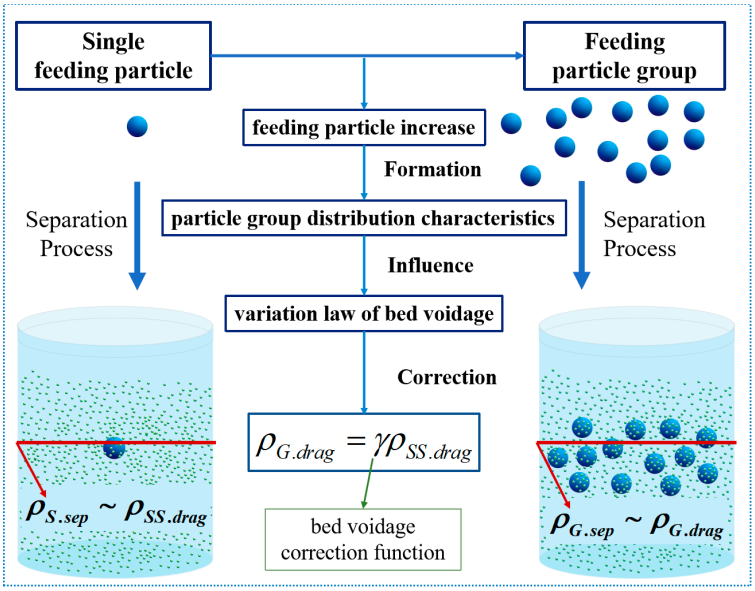


Figure 2. Schematic diagram of separation behavior of feeding group particle in gas–solid separation fluidized bed.

3.1. Density Prediction Model of Spherical Single Feeding Particle

Due to changes in the bed composition when the feeding particle group is introduced, the bed density also changes accordingly. Therefore, this study only focuses on the change between the separation density and bed density of the fluidized bed caused by the drag

force of the ascending gas flow when a single non-spherical particle is introduced, defined as $\rho_{S.drag}$. The calculation method for the $\rho_{S.drag}$ of non-spherical single particles when introduced can be obtained from previous research [24,25], as shown in Equation (1):

$$\left(\begin{array}{l} \rho_{S.drag} = \frac{F_d}{gV} = \frac{3C_D\rho_f\left(v_g - v_p\right)^2}{4gd_p} \\ C_D = \frac{24}{Re}\left(1 + C_4 Re^{C_5}\right) + C_6/\left(1 + C_7/Re\right) \\ C_4 = exp\left(2.33 - 6.46\Phi + 2.45\Phi^2\right) \\ C_5 = 0.096 + 0.556\Phi \\ C_6 = exp\left(4.90 - 13.89\Phi + 18.42\Phi^2 - 10.26\Phi^3\right) \\ C_7 = exp\left(1.47 + 12.26\Phi - 20.73\Phi^2 - 15.89\Phi^3\right) \end{array} \right) \quad (1)$$

Equation (1) primarily addresses the scenario where non-spherical single particles are introduced, taking into account the influence of the sphericity coefficient Φ on the $\rho_{S.drag}$. However, when dealing with a single-component particle group, it is also necessary to consider the interactions between the introduced particle groups, the interactions between the particle groups and the dense medium, as well as the impact of the bed voidage on the separation density. Therefore, in the research process, spherical particles are used as simulated particles to avoid the influence of the sphericity coefficient on the separation effect. When the introduced particles are spherical, the sphericity coefficient Φ is 1, and the calculation method for the $\rho_{SS.drag}$ in the case of a single spherical particle is shown in Equation (2):

$$\left(\begin{array}{l} \rho_{SS.drag} = \frac{F_d}{gV} = \frac{3C_{DS}\rho_f\left(v_g - v_p\right)^2}{4gd_p} \\ C_{DS} = \frac{24}{Re}\left(1 + 0.19Re^{0.65}\right) + 0.44/\left(1 + 1.15 \times 10^{-10}/Re\right) \end{array} \right) \quad (2)$$

Spherical single particles with different sizes and densities were feeding for separation experiments, and the predicted results for the $\rho_{SS.drag}$ are shown in Figure 3. From Figure 3, it can be seen that the prediction accuracy of using Equation (2) to predict the separation of spherical single particles when they are selected is over 80%. Therefore, Equation (2) can be used as a model for predicting the flow caused by the drag force of ascending airflow when single particles are selected in this study.

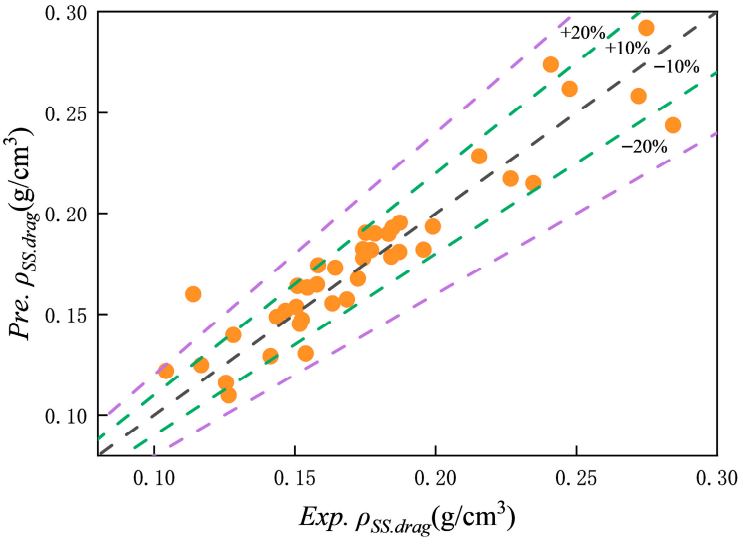


Figure 3. Prediction of the experimental results $\rho_{SS.drag}$ of spherical single feeding particle.

3.2. Bed Voidage

The bed voidage is calculated based on the Particle Segregation Model proposed by Alberto [26].

When the feeding particle group is in a suspended state in the fluidized bed, the density of the feeding particle group is the same as the bed separation density. At this time, the feeding particle group achieves force balance, and the resultant force it experiences is 0, as shown in Equation (3):

$$G_G + F_{Gf} + F_{Gd} = 0 \tag{3}$$

Based on the force balance of particles in the fluidized bed, it can be derived as shown in Equation (4):

$$\rho_{G.p}\frac{\pi}{6}d_p^3 g = \overline{\rho}(1-\varepsilon)\frac{\pi}{6}d_p^3 g + \varepsilon\overline{\rho}\frac{\pi}{6}d_p^2\overline{R}g \tag{4}$$

Define $\overline{\rho}$ as the average density, g/cm^3; $\overline{s}$ as the ratio of the density of the feeding particle group to the average density; and $\overline{R}$ as the ratio of the average particle size to the dense medium. The calculation formulas for $\overline{s}$ and $\overline{R}$ are shown in Equations (5) and (6):

$$\overline{s} = \frac{\rho_{G.p}}{\overline{\rho}} \tag{5}$$

$$\overline{R} = \frac{\overline{d}}{d_s} \tag{6}$$

The relationship between the feeding particle group and the void fraction related to the dense medium is shown in Equation (7) [26–28]:

$$\overline{s} = 1 - \varepsilon + \varepsilon\overline{d} \tag{7}$$

Among them, the calculations of the average density $\overline{\rho}$ and average particle size $\overline{d}$ of the feeding particles and magnetite dense medium are shown below from Equation (8) to (12):

$$\varphi_p = \frac{V_{G.p}}{V_{G.p} + V_s} \tag{8}$$

$$\varphi_s = \frac{V_s}{V_{G.p} + V_s} \tag{9}$$

$$\varphi_p + \varphi_s = 1 \tag{10}$$

$$\overline{\rho} = \varphi_p\rho_{G.p} + \varphi_s\rho_s \tag{11}$$

$$\overline{d} = \varphi_p d_{G.e} + \varphi_s d_s \tag{12}$$

where $V_{G.p}$ and V_s represent the volume of the feeding particle group and the dense medium, respectively. φ_p and φ_s represent the volume fractions of the feeding particle group and the dense medium, respectively.

This leads to the calculation method of voidage, as shown in Equations (13) and (14):

$$\varepsilon = \frac{\overline{s} - 1}{\overline{d} - 1} \tag{13}$$

$$\varepsilon = \frac{\frac{\rho_{G.p}}{\varphi_p\rho_{G.p} + \varphi_m\rho_m} - 1}{(\varphi_p d_{G.e} + \varphi_m d_m) - 1} \tag{14}$$

3.3. Bed Density Related to Feeding Particle Group

The expression for bed density is shown below [29]:

$$\rho_{bed} = 0.902\left\{\left[\rho_s \times \left(1-\varepsilon_{mf}\right) + \rho_g \times \varepsilon_{mf}\right](1-\varepsilon_b) + \rho_g\varepsilon_b\right\} \quad (15)$$

According to Equation (14), the density of the emulsion phase is related to the dense medium density ρ_s. Due to the addition of the feeding particle group, the average density $\overline{\rho}$ will replace the original bed density for the calculation, as shown in Equation (16):

$$\rho_{G.bed} = 0.902\left\{\left[\overline{\rho} \times \left(1-\varepsilon_{mf}\right) + \rho_g \times \varepsilon_{mf}\right](1-\varepsilon_b) + \rho_g\varepsilon_b\right\} \quad (16)$$

It can also be written as Equation (17):

$$\rho_{G.bed} = 0.902\left\{\left[\left(\varphi_p\rho_{G.p} + \varphi_m\rho_m\right) \times \left(1-\varepsilon_{mf}\right) + \rho_g \times \varepsilon_{mf}\right](1-\varepsilon_b) + \rho_g\varepsilon_b\right\} \quad (17)$$

3.4. Separation Density Related to Feeding Particle Group

In the gas–solid separation fluidized bed, the drag coefficient exerted by the airflow on the feeding particles is given by Equation (18):

$$Re_G = \frac{d_p v_g \rho_{G.f}}{\mu_{G.f}} \quad (18)$$

Meanwhile, the difference between the separation density and the bed density of the fluidized bed caused by the drag force of the upward airflow drag force during particle group fluidized bed separation is defined as $\rho_{G.drag}$, as shown in Equation (19):

$$\rho_{G.drag} = \frac{F_{G.d}}{gV} = \frac{3C_{G.D}\rho_f\left(v_{G.g} - v_{G.p}\right)^2}{4gd_e} \quad (19)$$

The formula for calculating the separation density at this time is shown in Equation (20):

$$\rho_{G.sep} = \rho_{G.bed} + \rho_{G.drag} \quad (20)$$

3.5. Measurement and Calculation of Experimental Particle Group Separation Density

Measure the position of each particle, and then measure the pressure drop at that point under the same conditions to obtain the density at that point. The average of the sum of the densities at each point is the separation density of the feeding particle group, as shown in Equation (21):

$$\rho_{G.(sep.\exp)} = \frac{\sum_{i=1}^{N} \frac{\Delta P}{g\Delta H}}{N} \quad (21)$$

4. Variation Law of Voidage and Density in the Feeding Group Particle Separation Process Under the Air Drag Force

4.1. Variation Law of Voidage and $\rho_{G\cdot drag}$ with the Number of Feeding Particles

This experiment had the following conditions: bed height at 120 mm and gas velocity at 0.148 m/s. The sphere feeding particle density is 2.0 g/cm^3. The number of feeding particles ranges from 5 to 30. As shown in Figure 4, with the increase in feeding particles, the voidage between particles gradually increases and remains between 50.05% and 50.15%. Due to the fact that the density of the feeding particles is lower than that of the dense medium, as the number of feeding particles increases, the average density decreases, while

the bed volume increases due to the addition of feeding particles, which leads to an increase in the bed voidage to a certain extent.

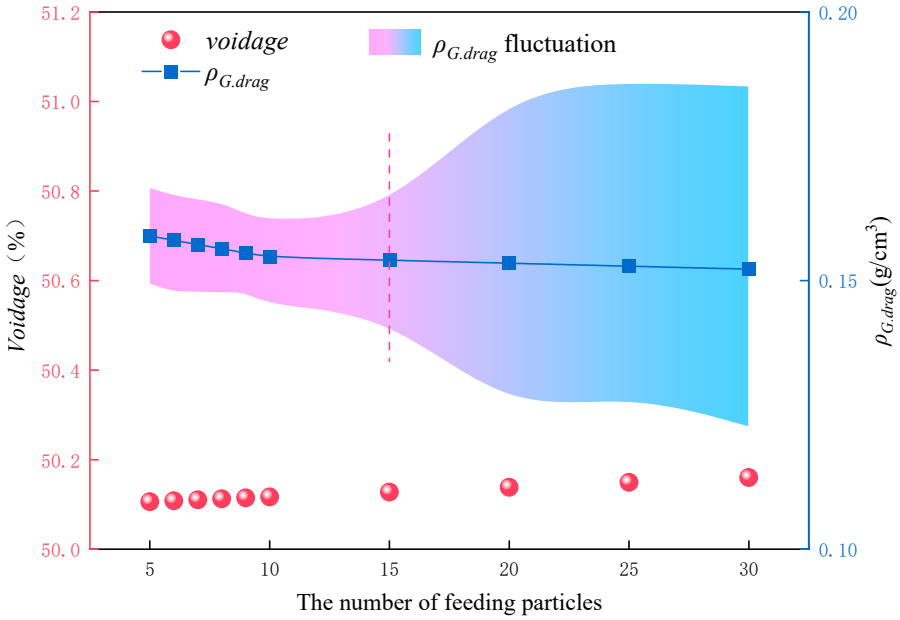


Figure 4. Variation law of voidage and $\rho_{G\cdot drag}$ with the number of feeding particles.

Figure 4 indicates that the voidage between the particles increases gradually with the increase in the feeding particles and the voidage between the particles is in a range of 50.05 to 50.15. Since the density of the feeding particles is lower than that of the dense medium, as the number of feeding particles increases, the average density reduces, and the bed volume rises from the addition of feeding particles, which causes an increase in the bed voidage to some extent.

As the number of feeding particles increases, the $\rho_{G\cdot drag}$ remains between 0.152–0.158 g/cm^3. However, with the increase in the number of feeding particles, the fluctuation in the $\rho_{G\cdot drag}$ significantly increases, indicating an increase in the fluctuation in the $\rho_{G\cdot drag}$. When the number of feeding particles is greater than 15, the fluctuation in the $\rho_{G\cdot drag}$ increases significantly, with the fluctuation range exceeding 0.1 g/cm^3. This is because with the addition of feeding particles, the stable separation environment originally established in the fluidized bed is impacted to some extent, the distribution of particles becomes more dispersed, and the feeding particles are more strongly influenced by the local environment. The increased number of collisions between feeding particles and particles in the emulsion phase medium, as well as the uneven distribution of local bubble phases, have a significant impact on the position of feeding particles, leading to their variability in position within the fluidized bed. Consequently, the fluctuation range of the $\rho_{G\cdot drag}$ increases when particles are feeding, and the error increases, reflecting a decrease in the stability of the bed with the increase in feeding particles.

4.2. Variation Law of Voidage and $\rho_{G\cdot drag}$ with the Density of Feeding Particles

This experiment had the following conditions: bed height at 120 mm and gas velocity at 0.148 m/s. The sphere feeding particle density ranges from 1.8 to 2.3 g/cm^3. The number of feeding particles was 10 and their diameter was 15 mm. As shown in Figure 5 the feeding particles with a density of 1.8 g/cm^3 float at the top of the fluidized bed, while the feeding particles with a density of 2.3 g/cm^3 sink to the bottom of the fluidized bed, indicating that the density of the fluidized bed is between the two. As the density of the feeding particles increases, the voidage also shows a gradually increasing trend, indicating that the density

of the feeding particles has a significant impact on the voidage. Particles with a density lower than the separation density are more difficult to sink and are located in the upper part of the fluidized bed, resulting in a lower voidage. Particles with densities between separation densities will be evenly distributed in the middle of the fluidized bed. During the sinking process, particles with a higher density are greatly affected by the unstable foaming and emulsion phase in the fluidized bed, resulting in uniform particle distribution and increased voidage.

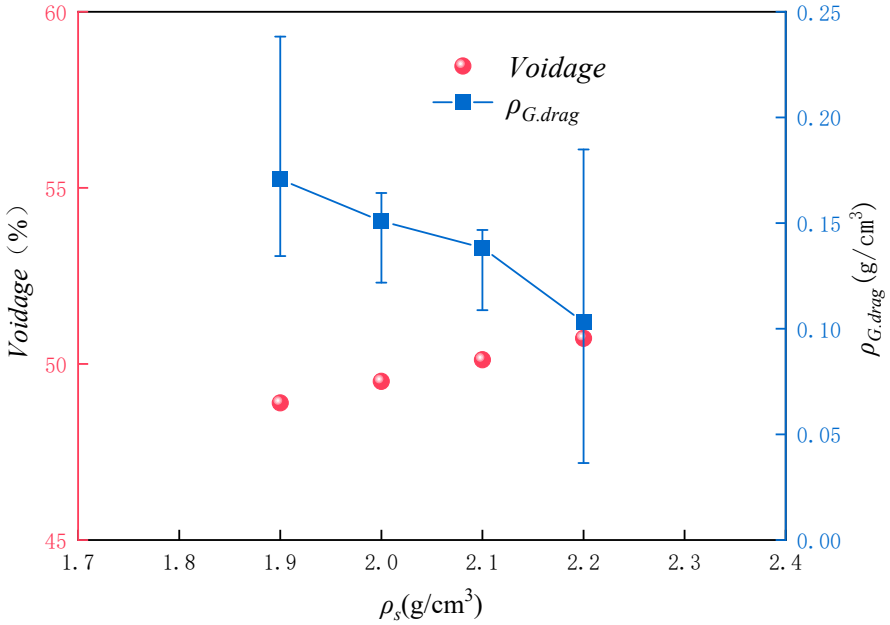


Figure 5. Variation law of voidage and $\rho_{G\cdot drag}$ with the density of feeding particles.

As the density of the feeding particles increases, the $\rho_{G\cdot drag}$ decreases. This indicates that as the density of the feeding particles increases, both the gravitational force and buoyancy force acting on the particles increase, while the drag force they experience in the fluidized bed decreases, resulting in a gradual decrease in the $\rho_{G\cdot drag}$. The larger errors in the $\rho_{G\cdot drag}$ obtained at 1.8 g/cm^3 and 2.2 g/cm^3 are due to the significant difference between the separation density and the bed density when calculating based on these densities, which leads to an increase in the error of the $\rho_{G\cdot drag}$.

4.3. Variation Law of Voidage and $\rho_{G\cdot drag}$ with the Size of Feeding Particles

This experiment had the following conditions: bed height at 120 mm and gas velocity at 0.148 m/s. The sphere feeding particle density was 2.0 g/cm^3. The number of feeding particles was 10, and their diameters ranged from 10 to 35 mm. As shown in Figure 6, as the particle size increased, the voidage gradually increased, remaining between 50.15% and 50.82%. With the decrease in particle size, under the same air velocity, the aerodynamic force per unit area on the particles increased, thus leading to an increase in the voidage of the particle group.

As the particle size of the feeding particle increases, the $\rho_{G\cdot drag}$ tends to decrease. This is because as the voidage increases, the drag coefficient of the particle group decreases to some extent. However, the overall change in the $\rho_{G\cdot drag}$ is not significant, ranging from 0.13 to 0.15 g/cm^3. This indicates that when the feeding particle size is greater than 15 mm, the separation effect in the fluidized bed is better. However, as the feeding particle size increases, the inertial effect of particle migration during the separation process becomes less significant, leading to more stable separation and reduced fluctuations in the $\rho_{G\cdot drag}$.

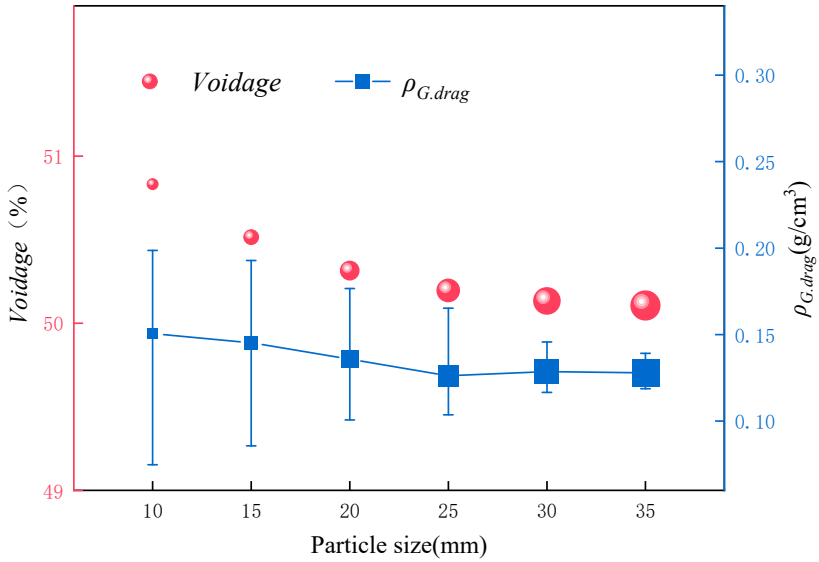


Figure 6. Variation law of voidage and $\rho_{G\cdot drag}$ with the size of feeding particles.

4.4. Variation Law of Voidage and $\rho_{G\cdot drag}$ with the Gas Velocity

This experiment had the following conditions: bed height at 120 mm and gas velocity between 0.14 and 0.18 m/s. The sphere feeding particle density is 2.0 g/cm^3. The number of feeding particles was 10 and their diameter was 15 mm. As shown in Figure 7, with the increase in gas velocity, the voidage of the bed also increases. The increase in gas velocity means that more gas enters the fluidized bed, leading to increased fluctuations in the bed, intensified particle movement within the bed, intense bubble movement, and faster merging of excess bubbles, resulting in an increase in bed voidage.

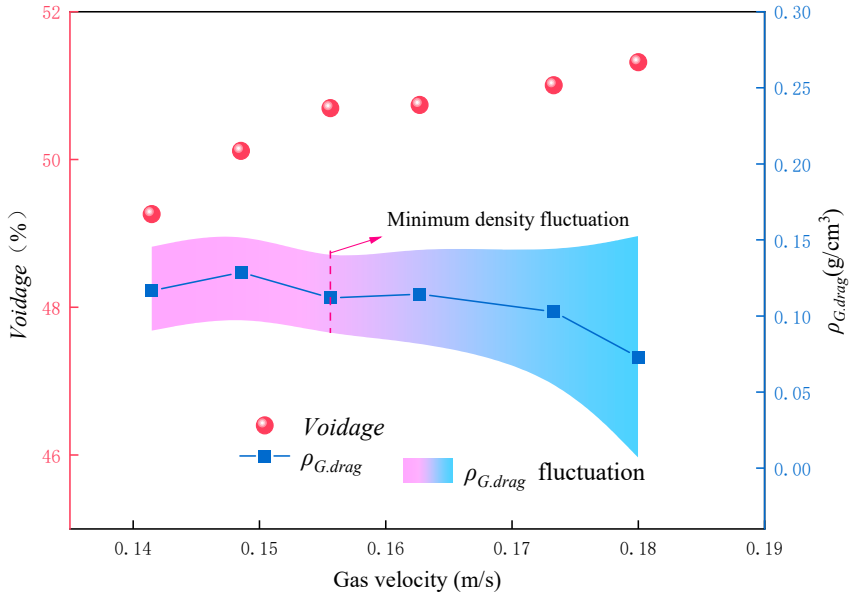


Figure 7. Variation law of voidage and $\rho_{G\cdot drag}$ with the gas velocity.

As the gas velocity increases, the proportion of bubbles in the fluidized bed increases, resulting in a decrease in the separation density of the bed and a reduction in the drag force on the particles. The $\rho_{G\cdot drag}$ of the particle group shows a decreasing trend. When the gas velocity increases, the fluctuation in the $\rho_{G\cdot drag}$ will first decrease and then increase. When the gas velocity is 0.155 m/s, the fluctuation in the $\rho_{G\cdot drag}$ is controlled within 0.047 g/cm^3, and the $\rho_{G\cdot drag}$ region is stable. But at the same time, with the increase in gas velocity, the

energy input increases, and the excess energy in the fluidized bed leads to the instability of the bed, while the error and fluctuation in the $\rho_{G\cdot drag}$ increase.

4.5. Variation Law of Voidage and $\rho_{G\cdot drag}$ with the Bed Height

This experiment had the following conditions: bed height between 80 and 160 mm, and gas velocity at 0.148 m/s. The sphere feeding particle density was 2.0 g/cm^3. The number of feeding particles was 10 and their diameter was 15 mm. As shown in Figure 8, with the increase in bed height, the voidage gradually and steadily increases. As the height of the bed increases, the upward airflow in the fluidized bed drives the expansion of dense medium to the bed. When the particle group enters the fluidized bed, it has a larger space for movement, providing more possibilities for the selection of particles. Therefore, the voidage of the particle group increases.

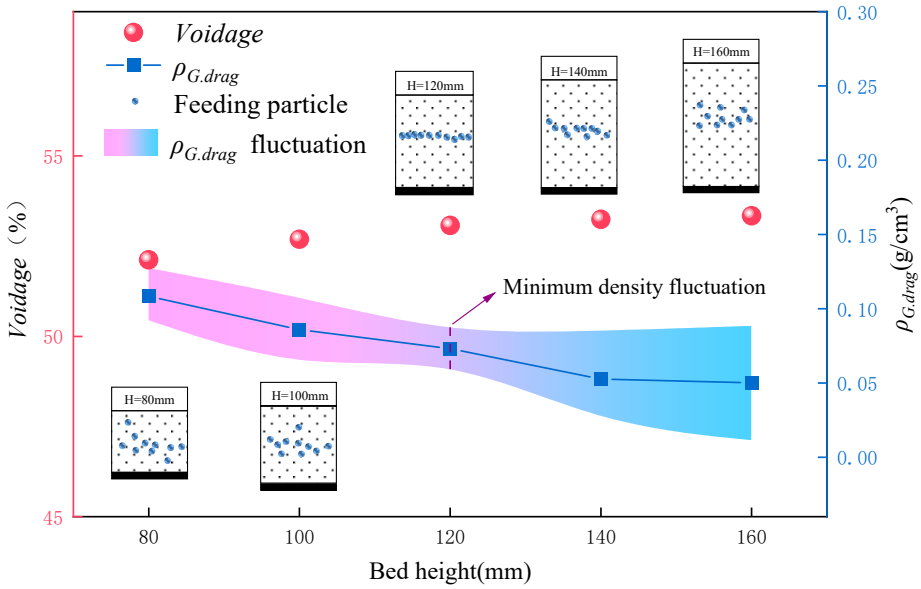


Figure 8. Variation law of voidage and $\rho_{G\cdot drag}$ with the bed height.

As the bed height increases, the $\rho_{G\cdot drag}$ tends to decrease. When the bed height is 120 mm, pressure fluctuations are minimal, and the $\rho_{G\cdot drag}$ remains relatively stable. When the bed height is optimized, the fluidization degree of the dense medium in the fluidized bed is higher, the bed activity further increases, the settling resistance of the dense medium to the particles decreases, and the pressure drop fluctuation from the top to bottom of the bed is lower, ensuring stable particle separation and smaller fluctuations in the $\rho_{G\cdot drag}$. As the bed height further increases, the possibility of bubbles merging to form larger bubbles increases. During the transfer of bubbles from the lower bed to the upper bed, they continue to merge and gradually increase in size, making it more prone to phenomena such as particle backmixing in the bed, and the disturbance to the bed gradually increases, leading to unstable fluctuations in bed pressure drop and increased fluctuations in the $\rho_{G\cdot drag}$.

4.6. Variation Law of Voidage and $\rho_{G\cdot drag}$ with the Distance Between Feeding Particles

Without considering the side wall effect, the distance between the feeding particles varies from 0 to 15 mm. Meanwhile, the diameter of the feeding particles is 15 mm. According to the experimental results shown in Figure 9, the distance between the feeding particles has almost no effect on the changes in the voidage and $\rho_{G\cdot drag}$ of the particle group after selection. The interactions between the feeding particle groups on the surface of the fluidized bed have little effect on their stratification and diffusion in the fluidized bed. The

change in the initial selection conditions when fluidized particles enter the fluidized bed means a difference in the initial voidage, but the physical properties of the feeding particle group have not undergone significant changes. According to the calculation of the above formula, the voidage of the feeding particle group has not changed. However, according to previous research, the change in the spacing between the feeding particle groups has no significant effect on the change in the drag coefficient of the particle group [21]. Therefore, the $\rho_{G\cdot drag}$ remains almost unchanged and remains in a stable range.

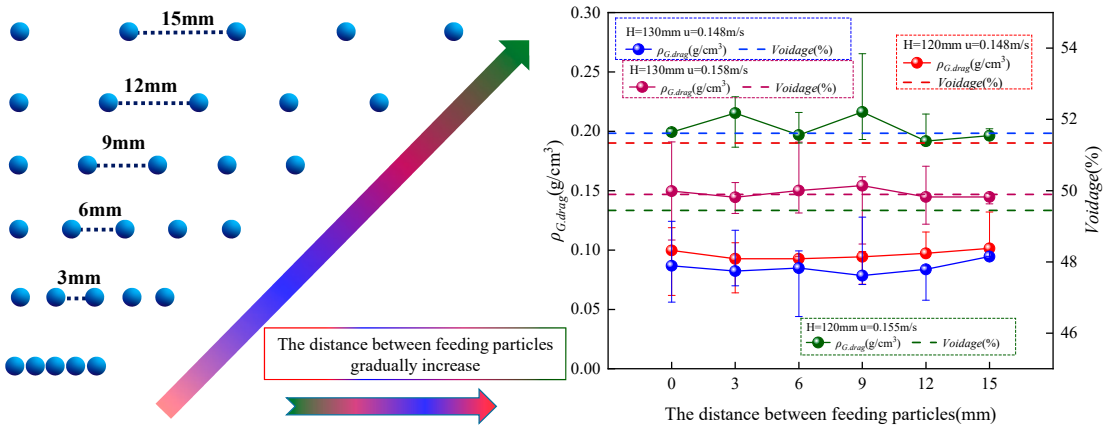


Figure 9. Variation law of voidage and $\rho_{G\cdot drag}$ with the distance between feeding particles.

5. Density Prediction Model and Error Analysis of Feeding Particle Group Under the Air Drag Force

5.1. The $\rho_{G\cdot drag}$ Prediction Model of Feeding Particle Groups

According to the results of the experiment, it can be concluded that under different conditions, the particle group voidage and particle group separation $\rho_{G\cdot drag}$ vary. Essentially, the change in particle group voidage leads to a change in the particle group drag coefficient, which in turn causes a change in the $\rho_{G\cdot drag}$. Therefore, the voidage can be used to correct the $\rho_{G\cdot drag}$ of the particle group.

Calculating the drag force experienced by feeding particle groups is challenging. Therefore, the $\rho_{SS\cdot drag}$ prediction model for a single feeding particle can be applied, with the introduction of a correction factor to study the situation of feeding particle groups. The $\rho_{G\cdot drag}$ for a feeding particle group and the $\rho_{SS\cdot drag}$ for a single feeding particle are as follows, where the coefficient γ is a correction function related to the void fraction, as shown in Equation (22):

$$\rho_{G.drag} = \gamma \rho_{SS.drag} \tag{22}$$

The relationship between the correction function related to the voidage and $\rho_{G\cdot drag}$ is illustrated in Figure 10. Based on the available experimental data, three fitting relationships with high correlation coefficients (R^2) are the exponential function, power function, and polynomial function, as shown in Equations (23)–(25):

$$\gamma = 4.915 \times 10^6 \times e^{-0.2997\varepsilon} \quad R^2 = 0.927 \tag{23}$$

$$\gamma = 9.232 \times 10^{25} \times \varepsilon^{-15.18} \quad R^2 = 0.926 \tag{24}$$

$$\gamma = 0.04753\varepsilon^2 - 5.201\varepsilon + 142.8 \quad R^2 = 0.926 \tag{25}$$

By analyzing the prediction accuracy of the three relational expressions, it can be concluded that when the prediction error of the power function of the $\rho_{G\cdot drag}$ prediction formula is 20%, the c confidence degree is 98.00%; when the prediction error of the power

function of the $\rho_{G\cdot drag}$ prediction formula is 10%, the confidence degree is 90.00%. Among the three prediction formulas, the power function has the highest prediction accuracy. Therefore, when selecting particle groups, the calculation formula for the $\rho_{G\cdot drag}$ is shown in Equation (26):

$$\rho_{G.drag} = \gamma\rho_{SS.drag} = 9.232 \times 10^{25} \times \varepsilon^{-15.18}\frac{3C_{DS}\rho_f(v_g - v_p)^2}{4gd_p} \quad (26)$$

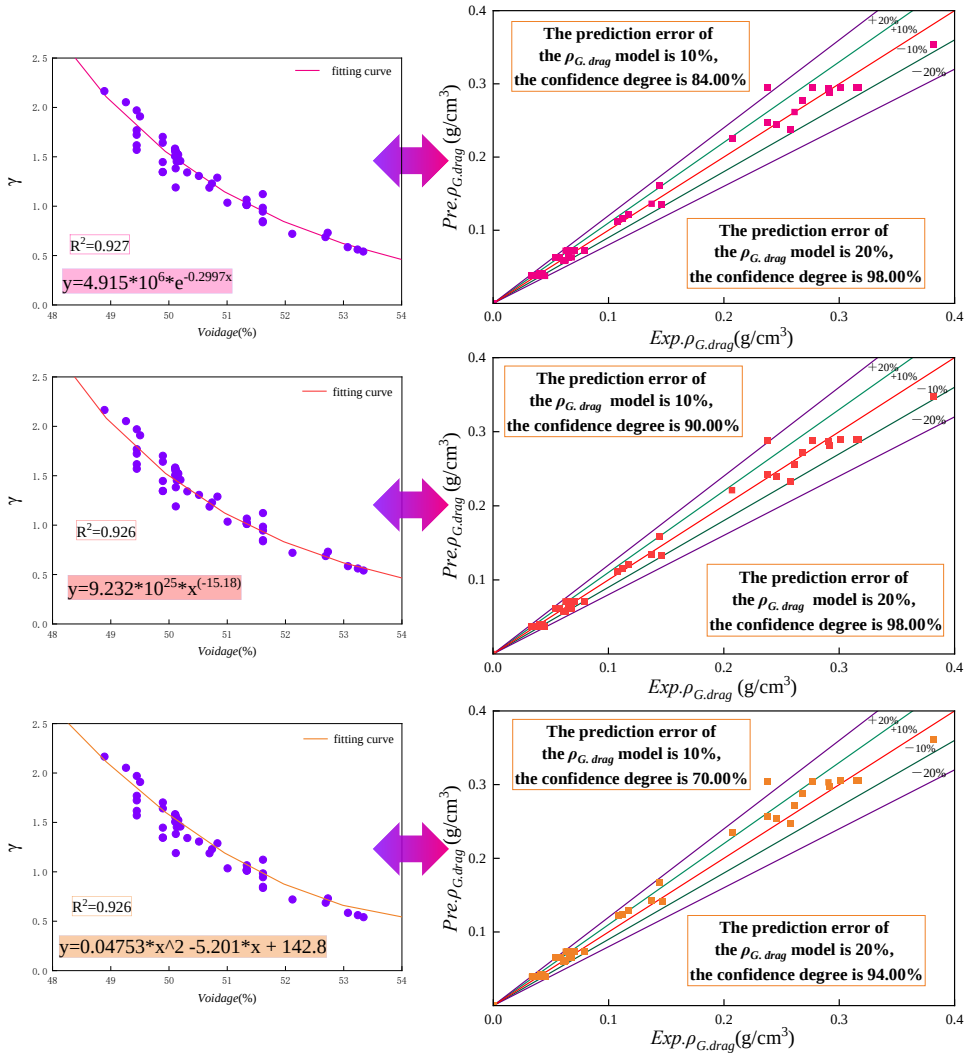


Figure 10. The relationship between voidage and the $\rho_{G\cdot drag}$.

5.2. Model Validation and Comparison of $\rho_{G\cdot drag}$

In the fluidized bed separation, few studies have investigated the changes in the $\rho_{G\cdot drag}$ during the separation of feeding particle groups, with the drag coefficient generally being the focus of correction. By comparing the accuracy of previous models involving the voidage and drag coefficient, we can further illustrate the accuracy of the $\rho_{G\cdot drag}$ prediction model proposed in this study during the introduction of feeding particle groups. The following three calculations of $\rho_{G\cdot drag}$ are compared when in the fluidized bed separation process.

The drag coefficient obtained by Yang [19] is further used to calculate the $\rho_{G\cdot drag}$, and the formula is shown in Equation (27):

$$\rho_{G.drag} = \left(-0.0101 + \frac{0.0038}{4(\varepsilon - 0.7463)^2 + 0.0040}\right)\rho_{SS.drag} \quad (27)$$

The drag coefficient obtained by Wen and Yu [20] is further used to calculate the $\rho_{G\cdot drag}$, and the formula is shown in Equation (28):

$$\rho_{G.drag} = \varepsilon^{-4.7}\rho_{SS.drag} \tag{28}$$

The drag coefficient obtained by Shen [21] is further used to calculate the ρG.drag, and the formula is shown in Equation (29):

$$\rho_{G.drag} = \left(44.62\varepsilon^2 - 85.81\varepsilon + 41.39\right)\rho_{SS.drag} \tag{29}$$

The predictive results of previous studies for the experimental results are shown in Figure 11. The drag coefficient models from previous studies exhibit poor predictive performance for the experimental results. Previous research has primarily focused on dilute-phase particles, typically with voidages exceeding 80%, and thus has limited predictive accuracy for the dense gas–solid separation fluidized bed with lower voidages. Therefore, the calculation formula for the voidage and $\rho_{G\cdot drag}$ proposed in this study holds significant guiding importance for the separation process in the gas–solid separation fluidized bed.

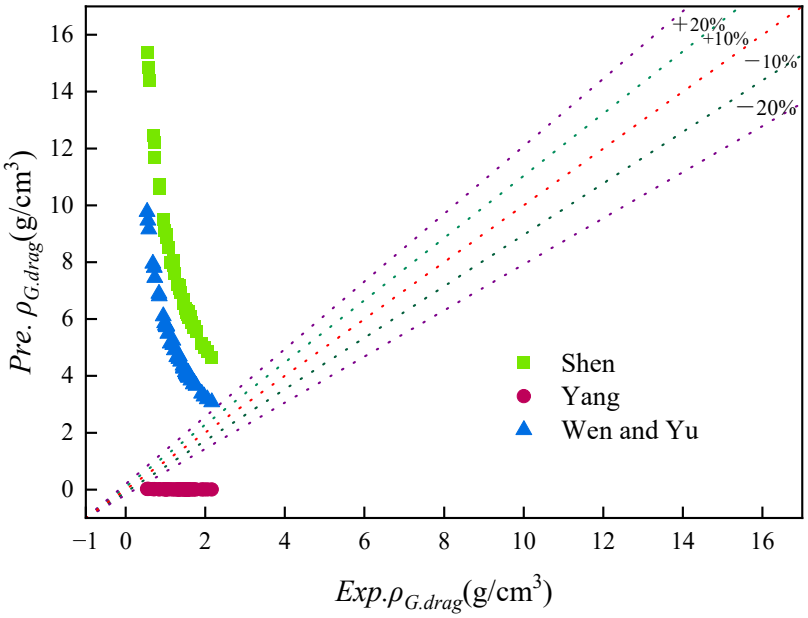


Figure 11. Prediction of the experimental results from previously modified formulas.

5.3. Verification of Separation Density of Non-Spherical Feeding Group Particle

By combining the separation density of single particles and the calculation method of $\rho_{G\cdot drag}$ when selecting a single-component spherical particle group, the separation density calculation method of a single-component spherical particle group is obtained, as shown in Equation (30), where the spherical coefficient of the particle group is replaced by the spherical coefficient (Φ) of non-spherical particles.

$$\left\{\begin{array}{l} \rho_{G.sep} = \rho_{G.bed} + \rho_{G.drag} \\ \rho_{G.bed} = 0.902\left\{\left[\left(\varphi_p\rho_{G.p} + \varphi_m\rho_m\right) \times \left(1 - \varepsilon_{mf}\right) + \rho_g \times \varepsilon_{mf}\right](1 - \varepsilon_b) + \rho_g\varepsilon_b\right\} \\ \rho_{G.drag} = 9.232 \times 10^{25} \times \varepsilon^{-15.18}\rho_{SS.drag} \end{array}\right\} \tag{30}$$

To verify the predictive accuracy of Equation (30), separation experiments were conducted using simulated particles such as cube, cuboid, and cylinder, with their main properties shown in Figure 12 below. The feeding cubes had sphericity coefficients of 0.42 and 0.45, cuboids had sphericity coefficients of 0.42 and 0.47, and cylinders had sphericity

coefficients of 0.42 and 0.51. The density of feeding particles is 2.1, 2.2, and 2.3 g/cm^3, and the number of feeding particles ranged from 8 to 10.

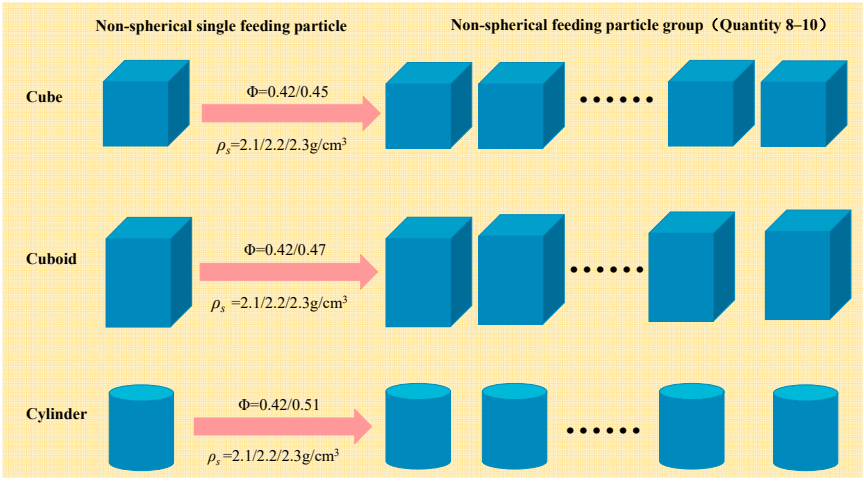


Figure 12. Schematic diagram of non-spherical feeding particle group.

The predicted separation density of a single-component non-spherical particle group is shown in Figure 13. As shown in this figure, the prediction error is controlled within 10%. Due to the complex and close relationship between the spherical coefficient of non-spherical particles feeding into the group and the arrangement of particles in the fluidized bed, it is difficult to quantitatively analyze the changes in the spherical coefficient from a single particle to a particle group, resulting in certain prediction errors. In summary, Equation (30) has a certain predictive effect on the separation density of single-component non-spherical particle groups, with a prediction accuracy of over 90%. It has important guiding significance for feeding particle group separation in the gas–solid separation fluidized bed.

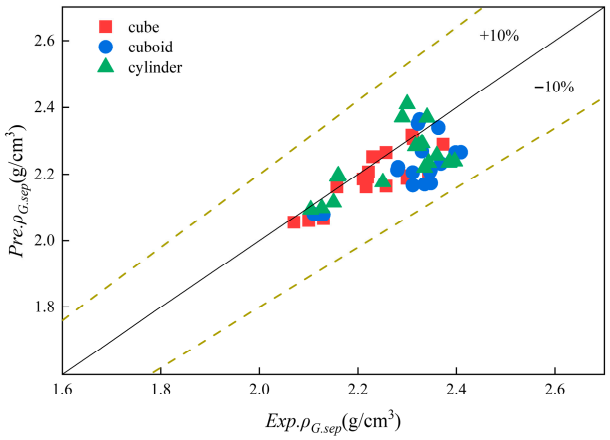


Figure 13. Prediction results of separation density of non-spherical feeding particle group.

6. Conclusions

This study investigates the separation rules of single-component feeding particle groups in the gas–solid separation fluidized bed. The conclusions are summarized as follows:

(1) The accuracy of the separation density prediction model for spherical single particles in the gas–solid separation fluidized bed is verified. A calculation method for bed voidage is introduced, and a theoretical calculation method for bed density and

separation density after the introduction of feeding particle group related to the bed voidage is established;

(2) The focus is on exploring the variation laws of the $\rho_{G\cdot drag}$ and voidage under a different bed height, gas velocity, number, particle density, size, and interparticle distance of the feeding particle group, and establishing the prediction model for the $\rho_{G\cdot drag}$ of the feeding particle group with the voidage as a correction factor;

(3) Based on the particle segregation model and the $\rho_{G\cdot drag}$ prediction model, the separation density prediction model for the single-component spherical feeding particle group in the gas–solid separation fluidized bed is obtained;

(4) Combined with the spherical coefficient, the separation density model is used to predict the separation density of single-component non-spherical feeding particle groups. The results show that this separation density model has important guiding significance for particle group separation in the gas–solid separation fluidized bed.

Author Contributions: Conceptualization, X.F.; Data curation, Y.H.; Formal analysis, Y.H.; Funding acquisition, X.F. and Y.F.; Project administration, L.S.; Resources, L.S.; Software, Y.H. and Y.L.; Supervision, X.F.; Validation, Y.F.; Writing—original draft, X.F., Y.F. and Y.L.; Writing—review and editing, X.F. and Y.L. All authors have read and agreed to the published version of the manuscript.

Funding: This research was funded by the Research Project Supported by Shanxi Scholarship Council of China (2024-128), the Taiyuan University of Science and Technology Scientific Research Initial Funding (20242017), the Fundamental Research Program of Shanxi Province (202403021212137, 202403021221136), the Award Fund for Outstanding Doctors in Shanxi Province (20242092), and the Scientific and Technological Achievements Transformation Guidance Project of Shanxi Province (202304021301046).

Data Availability Statement: The original contributions presented in this study are included in the article. Further in-quiries can be directed to the corresponding authors.

Acknowledgments: The authors wish to thank the Taiyuan University of Science and Technology, China University of Mining and Technology and Shanxi Province for support.

Conflicts of Interest: The authors declare no conflicts of interest.

Nomenclature

C_D	The drag coefficient
C_{DS}	The drag coefficient when a single spherical particle is introduced
$C_{G.D}$	The drag coefficient with feeding particle group
d_e	The equivalent diameter of feeding particle group, m;
d_s	The particle size of dense medium, m
$\overline{d}$	The average particle size, m
d_p	The equivalent diameter of coal particles, m; v_g is the velocity of the gas in the two-phase flow, m/s
F_d	The drag force of the gas experienced by the feeding particle in the fluidized bed, N
F_{Gf}	The buoyancy experienced by the feeding particle group in the fluidized bed, N
F_{Gd}	The drag force of the gas experienced by the feeding particle group in the fluidized bed, N
G_G	The gravity of the feeding particle group, N
g	The gravitational acceleration, m/s^2
ΔH	The height difference between different pressure measurement points, which is equivalent to the diameter of the sphere, m
N	The total number of feeding particles
ΔP	The pressure difference between different heights, Pa

Re	Reynolds number
Re_G	Reynolds number with feeding particle group
$\overline{R}$	The ratio of the average particle size to the dense medium
$\bar{s}$	The ratio of the density of the feeding particle group to the average density
V	The volume of fluidized bed, m^3
$V_{G.p}$	The volume of the feeding particle group, %
V_s	The volume of the dense medium, %
v_p	The velocity of the coal particles, m/s
$v_{G.g}$	The velocity of the gas in the two-phase flow with feeding particle group, m/s
$v_{G.p}$	The velocity of the coal particles with feeding particle group, m/s
Φ	The spherical coefficient of the feeding particle
ε	The voidage of fluidized bed, %
φ_p	The volume fractions of the feeding particle group, %
φ_s	The volume fractions of the dense medium, %
γ	The correction function related to the void fraction
ρ_f	The gas flow density, g/cm^3
$\rho_{SS.drag}$	The change in the difference between the separation density and bed density of the fluidized bed caused by the drag force of the ascending gas flow when a single spherical particle is introduced, g/cm^3
$\rho_{G.p}$	The density of feeding particle group, g/cm^3
$\overline{\rho}$	The average density, g/cm^3
ρ_{bed}	The density of fluidized bed, g/cm^3
ρ_s	The density of dense medium, g/cm^3
ε_{mf}	The bed voidage at critical fluidization state, %
ε_b	The proportion of bubble phase, %
ρ_g	The airflow density, approximately equal to the air density, 1.29×10^{-3} g/cm^3
$\rho_{G\cdot bed}$	The density of fluidized bed with feeding particle group, g/cm^3
$\rho_{G\cdot f}$	The gas flow density with feeding particle group, g/cm^3
$\mu_{G\cdot f}$	The viscosity with feeding particle group, Pa.S
$\rho_{G\cdot sep}$	The separation density of fluidized bed with feeding particle group, g/cm^3
$\rho_{G\cdot(sep.exp)}$	The experimental separation density of fluidized bed with feeding particle group, g/cm^3
$\rho_{S.drag}$	The change in the difference between the separation density and bed density of the fluidized bed caused by the drag force of the ascending gas flow when a single non-spherical particle is introduced, g/cm^3

References

1. Wang, C.; Liu, H.; Zhang, Y.; Zou, C.; Anthony, E.J. Review of arsenic behavior during coal combustion: Volatilization, transformation, emission and removal technologies. *Prog. Energy Combust.* **2018**, *68*, 1–28. [CrossRef]
2. Hower, J.C.; Groppo, J.G.; Graham, U.M.; Ward, C.R.; Kostova, I.J.; Maroto-Valer, M.M.; Dai, S. Coal-derived unburned carbons in fly ash: A review. *Int. J. Coal Geol.* **2017**, *179*, 11–27. [CrossRef]
3. Zhou, E.H.; Lu, J.Y.; Wang, Q.Q.; Lv, G.N.; Zhao, Y.M.; Dong, L.; Duan, C.L. Mixing and migration rule of binary medium in vibrated dense medium fluidized bed for fine coal separation. *Adv. Powder Technol.* **2020**, *31*, 3420–3432. [CrossRef]
4. Song, S.L.; Xu, X.; Tian, Y.K.; Chen, Z.Q. Study on density distribution characteristics and fine coal separation of magnetically fluidized beds of microfine particles. *Int. J. Coal Prep. Util.* **2024**, *44*, 1864–1879. [CrossRef]
5. Wang, J.M.; Jia, L.; Wang, Y.Y.; Wang, P.; Huang, L. Diffusion of "dual carbon" policies among Chinese cities: A network evolution analysis. *Energy* **2024**, *300*, 131514. [CrossRef]
6. Chen, Y.; Zhang, X.L.; Ji, J.; Zhang, C.X. Cold chain transportation energy conservation and emission reduction based on phase change materials under dual-carbon background: A review. *J. Energy Storage* **2024**, *86*, 111258. [CrossRef]
7. Zhu, H.T.; Cao, S.; Su, Z.M.; Zhuang, Y.; Zhang, X. China's future energy vision: Multi-scenario simulation based on energy consumption structure under dual carbon targets. *Energy* **2024**, *301*, 131751. [CrossRef]

8. Zhang, C.H.; Wang, Z.H.; Li, Y.H.; Zhang, D.C.; Balezentis, T. Can green credit policy with dual-carbon targets make highly polluting enterprises "green": A micro-analysis of total factor productivity growth. *J. Environ. Manag.* **2024**, *367*, 121981. [CrossRef]
9. China National Coal Association. *2024 Annual Report on the Development of the Coal Industry*; China National Coal Association: Beijing, China, 2025.
10. Oshitani, J.; Tanaka, Z.; Trisakti, B. Evaluation of particle behavior in gas-solid fluidized bed composed of different size particles by measurement of apparent buoyancy. *J. Soc. Powder Technol. Jpn.* **2010**, *38*, 97–103. [CrossRef]
11. Higashida, K.; Rai, K.; Yoshimori, W.; Ikegai, T.; Tsuji, T.; Harada, S.; Oshitani, J.; Tanaka, T. Dynamic vertical forces working on a large object floating in gas-fluidized bed: Discrete particle simulation and Lagrangian measurement. *Chem. Eng. Sci.* **2016**, *151*, 105–115. [CrossRef]
12. Yoshida, M.; Oshitani, J.; Tani, K.; Gotoh, K. Fluidized Bed Medium Separation (FBMS) using the particles with different hydrophilic and hydrophobic properties. *Adv. Powder Technol.* **2011**, *22*, 108–114. [CrossRef]
13. Oshitani, J.; Kiyoshima, K.; Tanaka, Z. Continuous dry material separation from automobile shredder residue. *Kagaku Kogaku Ronbun* **2003**, *29*, 8–14. [CrossRef]
14. Wang, Q.; Lu, J.; Yin, W.; Yang, H.; Wei, L. Numerical study of gas-solid flow in a coal beneficiation fluidized bed using kinetic theory of granular flow. *Fuel Process. Technol.* **2013**, *111*, 29–41. [CrossRef]
15. Wang, Q.; Feng, Y.; Lu, J.; Yin, W.; Yang, H.; Witt, P.J.; Zhang, M. Numerical study of particle segregation in a coal beneficiation fluidized bed by a TFM-DEM hybrid model: Influence of coal particle size and density. *Chem. Eng. J.* **2015**, *260*, 240–257. [CrossRef]
16. Wang, Q.; Yang, H.; Feng, Y.; Witt, P.J.; Lu, J.; Yin, W.; Liu, Q.; Wei, L. Numerical study of the effect of operation parameters on particle segregation in a coal beneficiation fluidized bed by a TFM-DEM hybrid model. *Chem. Eng. Sci.* **2015**, *131*, 256–270. [CrossRef]
17. Prusti, P.; Sahu, A.K.; Biswal, S.K. Prediction of the position of coal particles in an air dense medium fluidized bed system. *Int. J. Min. Sci. Technol.* **2015**, *25*, 421–427. [CrossRef]
18. Luo, Z.; Zhao, Y. *Separation Theory of Fluidization*; China University of Mining and Technology Press: Xuzhou, China, 2002.
19. Yang, N.; Wang, W.; Ge, W.; Li, J. CFD simulation of concurrent-up gas–solid flow in circulating fluidized beds with structure-dependent drag coefficient. *Chem. Eng. J.* **2003**, *96*, 71–80. [CrossRef]
20. Wen, C.Y.; Yu, Y.H. Mechanics of fluidization. *Chem. Eng. Prog. Symp. Ser.* **1966**, *62*, 100–111.
21. Zhiheng, S.; Hongwen, M.; Huilin, L.; Tingyu, S.; Zheng, L. Numerical Simulation and Application of Drag Coefficient of Particle Clusters in a Riser Based on Lattice-Boltzmann Method. *Petrochem. Technol.* **2012**, *41*, 544–550.
22. Ding, J.; Gidaspow, D. A bubbling fluidization model using kinetic theory of granular flow. *Aiche J.* **1990**, *36*, 523–538. [CrossRef]
23. Dingrong, B.; Yong, J. The Interaction Between Gas and Particlesin a Vertical Gas-Solid Flow System. *Ciesc J.* **1991**, *42*, 697–703.
24. Fan, X.C.; Fu, Y.P.; He, Y.L.; Sun, L.Y. Study on Separation Kinetics of Non-Spherical Single Feeding Particle in the Gas-Solid Separation Fluidized Bed. *Separations* **2024**, *11*, 341. [CrossRef]
25. Haider, A.; Levenspiel, O. Drag coefficient and terminal velocity of spherical and nonspherical particles. *Powder Technol.* **1989**, *58*, 63–70. [CrossRef]
26. Di Renzo, A.; Di Maio, F.P.; Girimonte, R.; Vivacqua, V. Segregation direction reversal of gas-fluidized biomass/inert mixtures—Experiments based on Particle Segregation Model predictions. *Chem. Eng. J.* **2015**, *262*, 727–736. [CrossRef]
27. Di Maio, F.P.; Di Renzo, A.; Vivacqua, V. A particle segregation model for gas-fluidization of binary mixtures. *Powder Technol.* **2012**, *226*, 180–188. [CrossRef]
28. Di Maio, F.P.; Di Renzo, A.; Vivacqua, V. Extension and validation of the particle segregation model for bubbling gas-fluidized beds of binary mixtures. *Chem. Eng. Sci.* **2013**, *97*, 139–151. [CrossRef]
29. Fan, X. *Study on Flow Pattern Transition and Separation Density in the Gas-Solid Separation Fluidized Bed*; China University of Mining and Technology: Xuzhou, China, 2022.

Disclaimer/Publisher's Note: The statements, opinions and data contained in all publications are solely those of the individual author(s) and contributor(s) and not of MDPI and/or the editor(s). MDPI and/or the editor(s) disclaim responsibility for any injury to people or property resulting from any ideas, methods, instructions or products referred to in the content.